

A CLAS Proposal for PAC44

Transition Form Factors of the η' and ϕ Mesons with CLAS12

M. C. Kunkel^{*†1}, M. J. Amarian², D. Lersch¹, J. Ritman^{†1}, S.
Schadmand^{†1}, X. Song¹

¹Forschungszentrum Jülich, Jülich (Germany)

²Old Dominion University (U.S.A.)

Abstract

Dalitz decays are radiative decays in which the photon is virtual and subsequently produces an electron positron pair, $P \rightarrow l^+l^-X$. Such decays serve as an important tool used to reveal the internal structure of hadrons and the interaction mechanisms between photons and hadrons. Furthermore, assuming point-like particles, the electromagnetic interaction is calculable within QED by the Kroll-Wada formula. Transition form factors quantify deviations from the QED decay rate. They characterize modifications of the point-like photon-meson vertex due to the structure of the meson. For the η' meson this deviation represents the internal structure of the meson, while for the ϕ meson the deviation represents the transition from $\phi \rightarrow \eta$. The transition form factor can be characterized as $|F(q^2)|$, where q^2 is the square of the invariant mass of the lepton pair, and can be determined by comparing QED predictions to the experimentally measured rate.

Measurements with the highest scientific impact on the determination of the transition form factor have been performed in the space-like region ($q^2 < 0$) in collider experiments. However, due to experimental limitations (e.g. π^\pm contamination in lepton sample, low branching fractions, external conversion contamination), transition form factors in the time-like region ($q^2 > 0$) have not yet been precisely determined. Recent measurements of the time-like transition form factor for $\eta' \rightarrow e^+e^-\gamma$ have been performed by the BESIII collaboration with insufficient statistical precision, therefore the proper theoretical description cannot be determined.

From previous CLAS analyses using the g12 data set, it was preliminarily shown that measurements of the time-like transition form factor were achievable, but without the statistical precision needed to be competitive. Therefore, we propose to use CLAS12 to focus

^{*}Contact person, email: m.kunkel@fz-juelich.de

[†]Spokesperson

on the dilepton decay channels from the reactions $ep \rightarrow e'p\eta'$ and $ep \rightarrow e'p\phi$, where $\eta' \rightarrow e^+e^-\gamma$ and $\phi \rightarrow \eta e^+e^-$. The CLAS12 detector will be used to identify and measure the e^+e^- decay products by means of the High Threshold Cherenkov Counter (HTCC), Pre-Calorimeter (PCAL) and Electromagnetic Calorimeter (EC). The combination of HTCC+PCAL+EC can provide a rejection factor for single e^\pm/π^\pm of up to 10^6 for momenta less than 4.9 GeV/c with $\approx 100\%$ efficiency. For dileptons (e^+e^- pairs), this rejection factor will be $\approx 10^{12}$, which enables dilepton studies for branching ratios $\approx 10^{-9}$. Precise determination of momenta and angles of the e^+e^- decay products are the key features available to CLAS12. The momentum and angle of final state photons will be determined in CLAS12 by using the PCAL and EC. Consequently, the photon in the process $\eta' \rightarrow e^+e^-\gamma$ and the photons in the process $\phi \rightarrow e^+e^-\eta \rightarrow e^+e^-\gamma\gamma$ will be detected. Preliminary studies using the CLAS12 simulation suite have shown that a beam time of 100 days, at full luminosity, will accumulate a data sample at least one order of magnitude larger in statistics than the most current $\eta' \rightarrow e^+e^-\gamma$ and $\phi \rightarrow \eta e^+e^-$ measurement.

Contents

| | | |
|----------|---|-----------|
| 1 | Introduction | 3 |
| 2 | Motivation | 4 |
| 3 | Kinematics | 4 |
| 3.1 | The Dalitz Decay | 6 |
| 3.2 | Form Factor | 6 |
| 3.3 | Photon Conversion to e^+e^- Pairs | 7 |
| 3.4 | Summary | 9 |
| 4 | Measurement | 10 |
| 4.1 | Previous CLAS analyses | 11 |
| 4.2 | Simulating and Reconstruction | 13 |
| 4.2.1 | Reconstruction And Acceptance | 13 |
| 4.3 | Calculating Expected Yield | 16 |
| 4.3.1 | Calculating Photon Flux | 16 |
| 4.3.2 | Calculating Yield | 17 |
| 4.4 | Realistic Yield | 18 |
| 4.5 | Acceptance at 100% Torus field | 19 |
| 5 | Manpower | 20 |
| 6 | Beam Time Request | 20 |
| | BIBLIOGRAPHY | 21 |

1 Introduction

In the year 1951, Richard Dalitz published a letter [1] in which he calculated the rate for the π^0 decaying into an electron-positron pair (dilepton) and a photon, $\pi^0 \rightarrow e^+e^-\gamma$. The calculation assumed that the decay proceeded through a two-photon decay in which one of the photons was virtual and converted internally into an electron-positron pair. This kind of reaction is now known as a Dalitz decay. The experimental evidence of this decay process was first observed in emulsion plates exposed to the Chicago cyclotron in 1952 [2] and a number of experiments performed over the next ten years verified Dalitz's hypothesis that the $\pi^0 \rightarrow e^+e^-\gamma$ decay resulted from internal conversion of a virtual photon [3, 4, 5]. A few years later N. Kroll and W. Wada calculated the framework for Dalitz decays within the QED framework [6], and extended the framework to double Dalitz Decays, in which the π^0 decays into two electron-positron pairs via emission of two virtual photons. Throughout the following years, much work was done to extend the framework of Dalitz decays to heavier mesons, such as η , ω , η' , and ϕ . With numerous experimental data taken, it was shown that the shape of the dilepton mass spectrum deviated from the QED predictions. Such deviations are attributed to the meson not being point-like, as calculated in QED, but instead to the internal structure of the meson. The virtual photon, that decayed into a dilepton pair, has the ability to probe the structure of meson because, like its on-shell counterpart, emission of a virtual photon is radiation, which decouples from any strong interaction within the meson when the meson transitions into its decay. Therefore, the information of the transition is encoded into the virtual photon, known as the Transition Form Factor (TFF), and can be characterized as $|F(q^2)|$, where q^2 is the square of the invariant mass of the lepton pair. The transition form factor can be determined by comparing QED predictions to the experimentally measured rate.

In this proposal we present an experiment to study two channels of which decay via Dalitz decays, $\eta \rightarrow e^+e^-\gamma$ and $\phi \rightarrow e^+e^-\eta$. The η and ϕ are produced via electro-production, $ep \rightarrow ep\eta'$ and $ep \rightarrow ep\phi$ in Hall B, using the CLAS12 detector. The superior $e^+e^-/\pi^+\pi^-$ discrimination of the CLAS12 detector will give access to measurements for which $e^+e^-/\pi^+\pi^-$ branching ratios of 10^{12} is achievable. This proposal is organized as follows. In Section 2 we summarize the current knowledge of Dalitz decays and transition form factors, challenges in dilepton signal quality and how the CLAS12 detector can surpass the current challenges in measuring a TFF of low statistical error. In Section 3, an explanation of the kinematics of the decay processes will be given as well as kinematics of main competing backgrounds. In Sec-

tion 4 a brief discussion on past CLAS analysis will be given, along with a description of analysis techniques that have been used and will be used in a CLAS12 measurement. Also in Section 4, an explanation of the Monte-Carlo simulations that were performed to extract the acceptances will be given as well as a calculation of expected yield and a validity check on the expected yield from previous CLAS analyses. In Section ?? we present the beam time request and a summary of the experiment.

2 Motivation

Here I will briefly write about the motivation to use dalitz decays to study the structure of meson. I will include the g-2 measurements Previous results etc

3 Kinematics

The two channels proposed to be studied are

$$e(k) + p(p) \rightarrow e'(k') + p'(p') + \eta'(\nu) \quad (1)$$

$$e(k) + p(p) \rightarrow e'(k') + p'(p') + \phi(\nu) , \quad (2)$$

where k, k', p, p' are the four-momenta of the incident lepton, outgoing lepton, target proton and scattered proton respectively. The virtual photon in the production is defined as $q = k - k'$ with energy $v = \frac{pq}{m_p} = E - E'$. The quantities $\eta'(\nu)$ and $\phi(\nu)$ are the electro-produced mesons. The production mechanisms of such mesons have been already proposed in previous proposals [7, 8] and are scheduled to run in conjunction with RunGroupA, the same run group requested for in this proposal. The main decays studied for this proposal are:

$$\eta' \rightarrow \gamma\gamma \rightarrow e^+e^-\gamma \quad (3)$$

$$\eta' \rightarrow \gamma\gamma^* \rightarrow \gamma e^+e^- \quad (4)$$

i.e. when a pseudoscalar meson, $P_p(\eta')$, decays via two photons (Eq. 3) and one photon converts into an e^+e^- pair due to E.M. processes through matter, this is conventionally known as external conversions. This decay channel will be the main background contribution and is further discussed in SecXXX. The Dalitz decay, or internal conversion, is when the $P_p(\eta')$ decays via a real photon and a virtual photon (Eq. 4), which decays into an e^+e^- pair.

$$\phi \rightarrow \eta\gamma \rightarrow \eta e^+e^- \quad (5)$$

$$\phi \rightarrow \eta\gamma^* \rightarrow \eta e^+e^- , \quad (6)$$

i.e. when a vector meson $V_p(\phi)$, decays via an η and a photon (Eq. 5) and one photon converts into an e^+e^- pair. The Dalitz decay for the ϕ is when

$V_p(\phi)$ decays via an η and a virtual photon (Eq. 6), which decays into an e^+e^- pair. Figure 1 illustrates the Feynman diagrams for the pseudoscalar “two photon decay” and “Dalitz decay”, while Fig. 2 illustrates the Feynman diagrams for the vector “pseudoscalar photon decay” and “Dalitz decay”. A

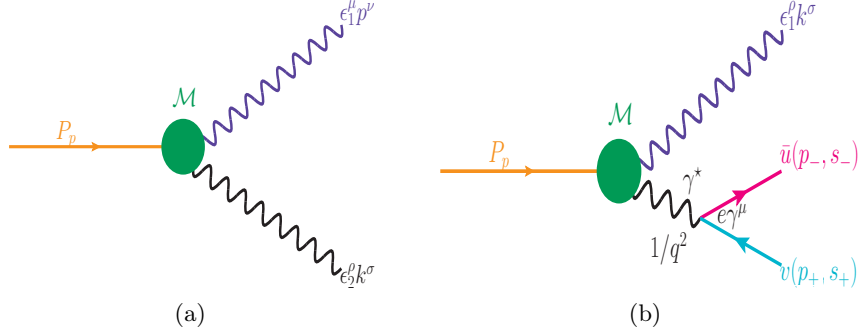


Figure 1: Feynman diagram of $P_p(\eta')$ two photon decay (a), ϵ_1 and ϵ_2 are the polarizations, p and k are 4-momenta of the photons. Feynman diagram of $P_p(\eta')$ Dalitz decay (b), the variable s_{\pm} are the spin helicities of the outgoing leptons l^{\pm} with 4-momenta p_{\pm} and ϵ is the polarization of the outgoing photon with 4-momenta k . In both diagrams \mathcal{M} is the form factor.

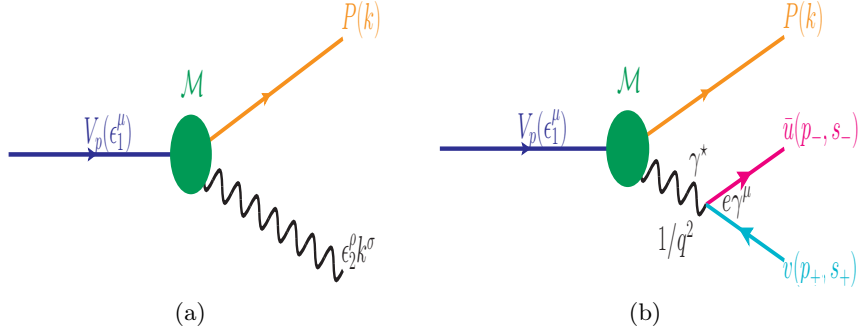


Figure 2: Feynman diagram of $V_p(\phi)$ decays. Notation same as in Fig. 1.

full derivation of the external conversion and Dalitz decay are given in the Appendix A.

3.1 The Dalitz Decay

The Dalitz decay of mesons is dependent on the spin of the meson. For pseudoscalar meson the decay rate is derived in A.3 and is expressed as:

$$\frac{d\Gamma_{e^+e^-\gamma}}{\Gamma_{\gamma\gamma}dq^2} = \frac{2\alpha}{3\pi} \frac{1}{q^2} \left(1 - \frac{q^2}{m_p^2}\right)^3 \left(1 + \frac{2m_l^2}{q^2}\right) \left(1 - \frac{4m_l^2}{q^2}\right)^{\frac{1}{2}} \quad (7)$$

which is the Kroll-Wada equation founded in [6, 9]. For vector mesons, the decay rate can be expressed as:

$$\frac{d\Gamma}{\Gamma_{\eta\gamma}dq^2} = \frac{\alpha}{3\pi} \frac{1}{q^2} \left(\left(1 + \frac{q^2}{m_\phi^2 - m_\eta^2}\right)^2 - \frac{4m_\phi^2 q^2}{m_\phi^2 - m_\eta^2} \right)^{\frac{3}{2}} \left(1 + \frac{2m_l^2}{q^2}\right) \left(1 - \frac{4m_l^2}{q^2}\right)^{\frac{1}{2}}, \quad (8)$$

as derived as [9]: An example of QED expectation for η' and ϕ is shown in Fig. 3.

3.2 Form Factor

The form factor $M_P(p^2, k^2 = 0)$ or $M_P(p_1^2, p_2^2)$ can be written as follows:

$$M_P \rightarrow M_P \times |F(q^2)|, \quad (9)$$

where M_P is the decay constant of two photons or η photon (as mentioned in Sec. A.1), while $|F(q^2)|$ is called the transition form factor, which defines the electromagnetic space structure of the meson, therefore for the $\eta' \rightarrow e^+e^-\gamma$ the decay rate modifies as;

$$\frac{d\Gamma_{e^+e^-\gamma}}{\Gamma_{\gamma\gamma}dq^2} = \frac{2\alpha}{3\pi} \frac{1}{q^2} \left(1 - \frac{q^2}{m_p^2}\right)^3 \left(1 + \frac{2m_l^2}{q^2}\right) \left(1 - \frac{4m_l^2}{q^2}\right)^{\frac{1}{2}} |F(q^2)|^2, \quad (10)$$

,which is the Kroll-Wada equation founded in [6], while the $\phi \rightarrow \eta e^+e^-$ decay rate modifies as;

$$\frac{d\Gamma_{\eta e^+e^-}}{\Gamma_{\eta\gamma}dq^2} = \frac{\alpha}{3\pi} \frac{1}{q^2} \left(\left(1 + \frac{q^2}{m_\phi^2 - m_\eta^2}\right)^2 - \frac{4m_\phi^2 q^2}{m_\phi^2 - m_\eta^2} \right)^{\frac{3}{2}} \left(1 + \frac{2m_l^2}{q^2}\right) \left(1 - \frac{4m_l^2}{q^2}\right)^{\frac{1}{2}} |F(q^2)|^2, \quad (11)$$

The value of $|F(q^2)|$ can be directly measured by comparison of the differential cross section with that of Q.E.D. pointlike differential cross section i.e.

$$\frac{d\sigma}{dq^2} = \left[\frac{d\sigma}{dq^2} \right]_{\text{pointlike}} |F(q^2)|^2,$$

or by performing a line shape analysis on the l^+l^- invariant system using assumptions on the structure of $|F(q^2)|$. One such assumption for $|F(q^2)|$ is the dipole approximation, from the Vector Dominance Model (VMD), in which

$$F(q^2) = \frac{\Lambda^2(\Lambda^2 + \gamma^2)}{(\Lambda^2 - q^2) + \Lambda^2\gamma^2}$$

where the parameters Λ and γ correspond to the mass and width of the Breit-Wigner shape for the effective contributing vector meson. A first approximation is that $\Lambda \approx M_\rho \approx 0.7$ GeV and $\gamma \approx \Gamma_\rho \approx 0.12$ GeV. A comparison showing the QED spectra and the deviation from QED using the VMD parameterization is shown in Fig. 3 for η' and ϕ .

3.3 Photon Conversion to e^+e^- Pairs

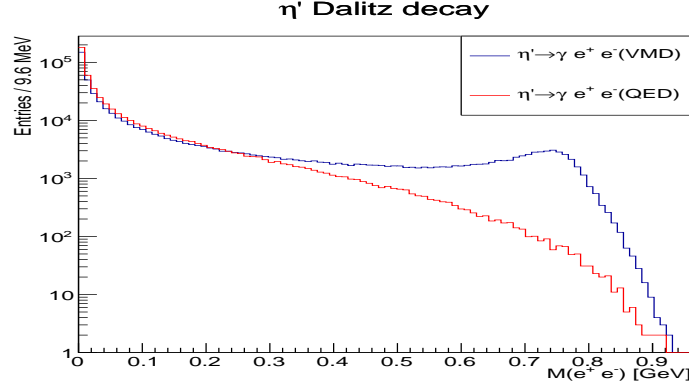
When a photon travels through matter at energies greater than 100 MeV, it can convert into an electron-positron pair. The process of pair production, $\gamma Z \rightarrow Ze^+e^-$, occurs when a photon with $E_0 > 2m_e c^2$ converts into an electron and a positron. The cross section for this process can be written as;

$$\sigma_{\gamma \rightarrow e^+e^-} = \frac{A}{N_A \rho \lambda_\gamma}, \quad \lambda_\gamma = \frac{9}{7} X_0 \quad (12)$$

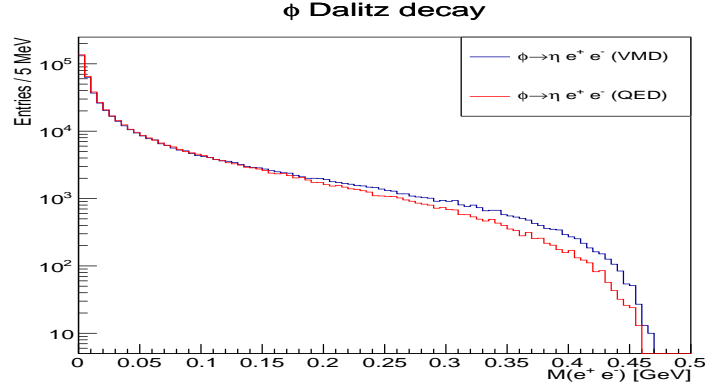
where λ is the interaction length, or mean free path, ρ is the density of the material, N_A is Avogadro's number and A is the atomic mass of the material. The probability of pair production to occur is solely based on X_0 , the radiation length of the medium and this probability can be expressed as;

$$\frac{dP}{dx} = \frac{1}{\lambda_\gamma} \exp\left(\frac{-x}{\lambda_\gamma}\right). \quad (13)$$

Using the ratio, $\frac{\Gamma_{\eta' \rightarrow e^+e^-\gamma}}{\Gamma_{\eta' \rightarrow \gamma\gamma}} = 2.13 \cdot 10^{-2}$, that has been preliminary measured by CLAS, which is consistent with [10], the probability of pair production when a photon, from the $\eta' \rightarrow \gamma\gamma$ decay, traveling through 5 cm of liquid hydrogen, ℓ_{H_2} , is shown in Fig. 4 as well as the number of $\eta' \rightarrow \gamma\gamma \rightarrow e^+e^-\gamma$ / $100\eta' \rightarrow e^+e^-\gamma$. Since CLAS12 has a vertex resolution of ≈ 1 mm the probability of pair production traveling through 10 mm is shown in Fig. 5. Therefore, a 1 mm cut on the primary vertex will yield a contamination of \approx one externally converted e^+e^- from $\eta' \rightarrow \gamma\gamma \rightarrow e^+e^-\gamma$ per Dalitz decays $100\eta' \rightarrow e^+e^-\gamma$. These type of subprocess mimics the Dalitz decay $\eta' \rightarrow e^+e^-\gamma$, described in Sec. A.3. Since there are two photons with equal probability of conversion for $\eta' \rightarrow \gamma\gamma$, the total probabilities shown is for when either photon externally converts. Using the ratio, $\frac{\Gamma_{\phi \rightarrow e^+e^-\eta}}{\Gamma_{\phi \rightarrow \gamma\eta}} = 9.58 \cdot 10^{-2}$ [11], the probability of pair production when a photon, from the $\phi \rightarrow \gamma\eta$ decay, traveling through 5 cm of liquid hydrogen, ℓ_{H_2} , is shown in Fig. 6 as well



(a)



(b)

Figure 3: Example of Dalitz spectra for η' using only QED(red) and the deviation from QED using the VMD parameterization(blue) with 500K Dalitz events generated (a). Example of Dalitz spectra for ϕ using only QED(red) and the deviation from QED using the VMD parameterization(blue) with 500K Dalitz events generated (b).

as the number of $\phi \rightarrow \gamma \eta \rightarrow e^+ e^- \eta$ / $100 \phi \rightarrow e^+ e^- \eta$. Since CLAS12 has a vertex resolution of ≈ 1 mm the probability of pair production traveling through 10 mm is shown in Fig. 5. Therefore, a 1 mm cut on the primary vertex will yield a contamination of \approx one externally converted $e^+ e^-$ from $\phi \rightarrow \gamma \eta \rightarrow e^+ e^- \eta$ per Dalitz decays $100 \phi \rightarrow e^+ e^- \eta$. From multiple scattering effects the $e^+ e^-$ from a converted photon will obtain a mass distribution. Simulations of photons from η' and ϕ radiative decays traversing through 1 mm of ℓH_2 show that the $e^+ e^-$ can obtain a maximum mass of ~ 0.14 GeV.

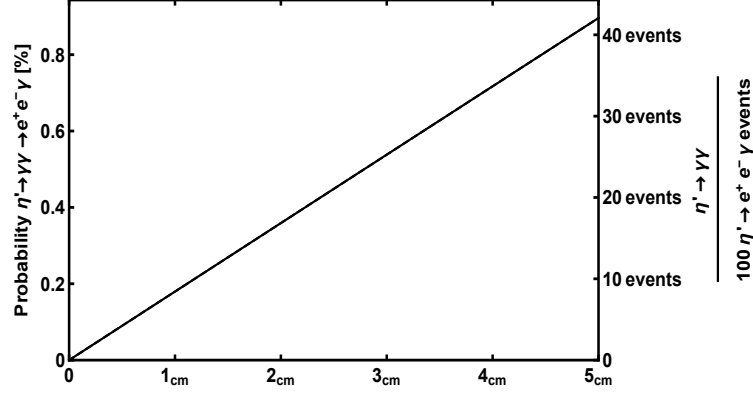


Figure 4: (Left axis) Probability of pair production, $\gamma \rightarrow e^+e^-$; (Right axis) number of $\eta' \rightarrow \gamma\gamma \rightarrow e^+e^-\gamma / 100\eta' \rightarrow e^+e^-\gamma$ as a function of distance in liquid hydrogen.

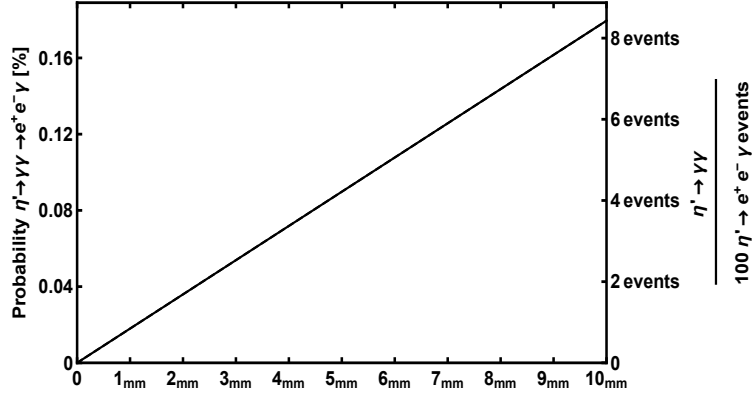


Figure 5: (Left axis) Probability of pair production, $\gamma \rightarrow e^+e^-$; (Right axis) number of $\eta' \rightarrow \gamma\gamma \rightarrow e^+e^-\gamma / 100\eta' \rightarrow e^+e^-\gamma$ as a function of distance in liquid hydrogen.

3.4 Summary

The $\gamma\gamma$ decay and the $\gamma^*\gamma$ decay have different branching ratios as do the decays $\gamma\eta$ decay and the $\gamma^*\eta$. This difference is attributed to the factor of α along with a q^2 dependence calculated in the Dalitz decay. However, due to the probability of a photon converting into an electron-positron pair in ℓH_2 , the total amount of e^+e^- pairs produced via photon conversion can contaminate the measurement of the form factor. The CLAS detector will have vertex resolution of ~ 1 mm, therefore the amount of contamination of externally converted pairs will be minimized by the vertex position of the

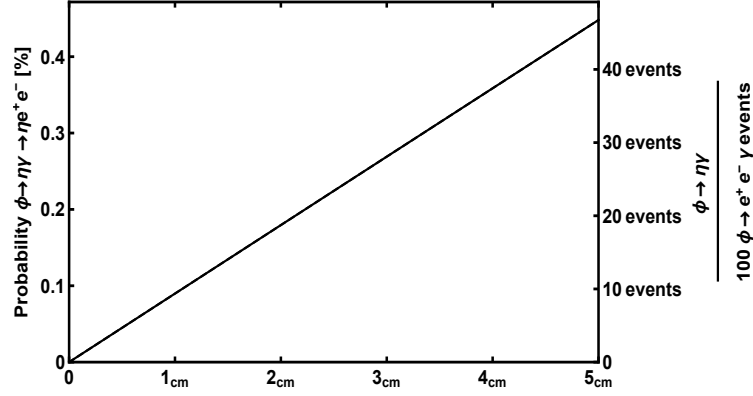


Figure 6: (Left axis) Probability of pair production, $\gamma \rightarrow e^+ e^-$; (Right axis) number of $\phi \rightarrow \gamma \eta \rightarrow e^+ e^- \eta$ / $100 \phi \rightarrow e^+ e^- \eta$ as a function of distance in liquid hydrogen.

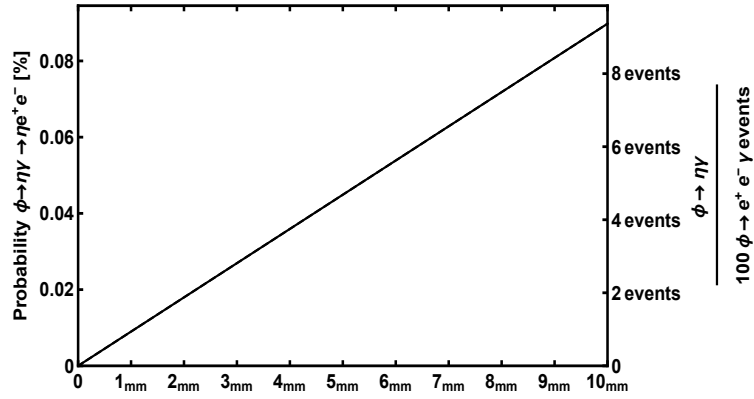


Figure 7: (Left axis) Probability of pair production, $\gamma \rightarrow e^+ e^-$; (Right axis) number of $\phi \rightarrow \gamma \eta \rightarrow e^+ e^- \eta$ / $100 \phi \rightarrow e^+ e^- \eta$ as a function of distance in liquid hydrogen.

$e^+ e^-$ pair. An example of the total contamination, in the Dalitz spectrum, from external conversion within 1 mm of the primary vertex can be seen in Fig. 9.

4 Measurement

This section will describe the previous CLAS preliminary result on the η' analysis performed with the g12 experiment. Also in this section is a description on how the $\eta \rightarrow e^+ e^- \gamma$ and $\phi \rightarrow e^+ e^- \eta$ were simulated and reconstructed for this CLAS12 proposal.

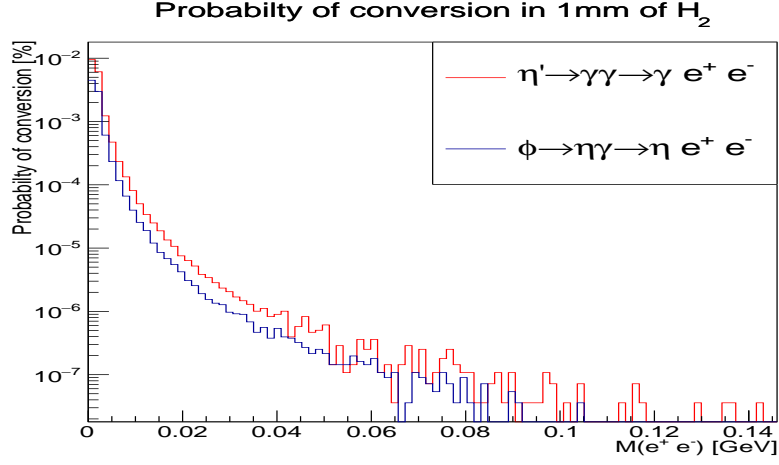


Figure 8: Probability of pair production in 1 mm of ℓH_2 for $\eta' \rightarrow \gamma\gamma$ and $\phi \rightarrow \gamma\eta$ vs. $M(e^+e^-)$

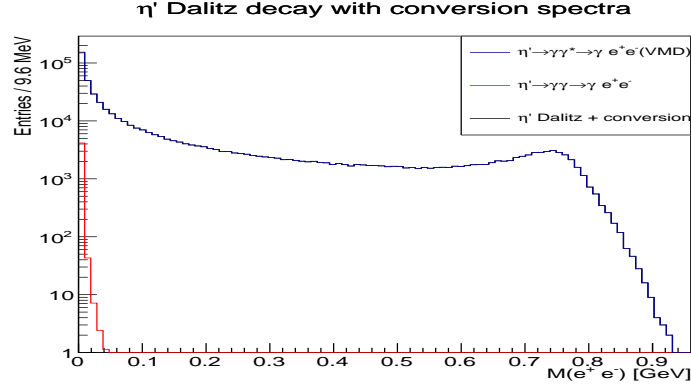
4.1 Previous CLAS analyses

The g12 experiment performed at CLAS produced data set of photon-induced reactions. Fortunately, the Cherenkov Counters(CC) were filled with per-flourbutane (C_4F_{10}) and a trigger consisting of a coincidence between the (ST·TOF)(CC·EC) allowing the study of dilepton reactions throughout the entire beam energy range $1.15 \text{ GeV} < E_\gamma < 5.45 \text{ GeV}$. Preliminary analyses of g12 involving dileptons include the decays:

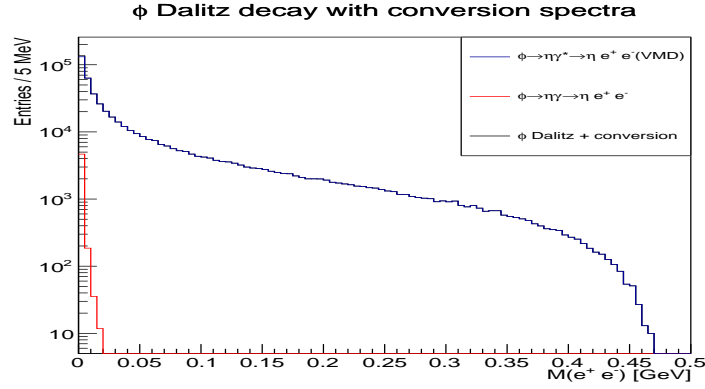
- $\Delta \rightarrow p e^+ e^-$ (Transition form factor)
- $\eta \rightarrow e^+ e^- \gamma$ (Transition form factor)

while advanced analyses involving dileptons include:

- $\pi^0 \rightarrow e^+ e^- \gamma$ (Differential Cross-Section)
- $\omega/\rho \rightarrow e^+ e^-$ (Interference of ω/ρ)
- $\omega \rightarrow e^+ e^- \pi^0$ (Transition form factor)
- $\eta' \rightarrow e^+ e^- \gamma$ (Transition form factor / branching ratio)

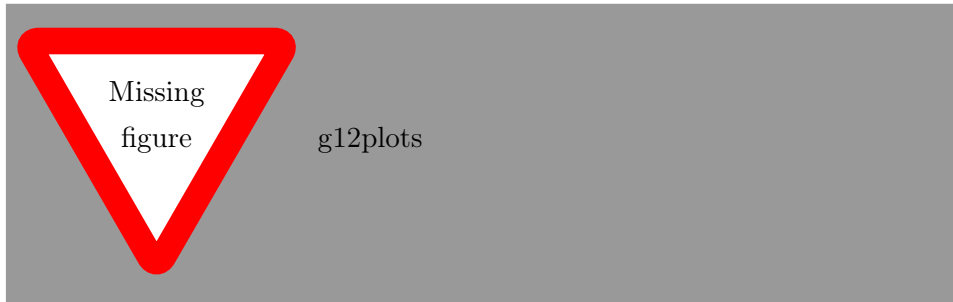


(a)



(b)

Figure 9: Example of Dalitz and conversion spectra for η' with 500K Dalitz events generated and $\sim 2.35 \cdot 10^7$ $\eta' \rightarrow \gamma\gamma$ generated (a). Example of Dalitz and conversion spectra for ϕ with 500K Dalitz events generated and $\sim 5.7 \cdot 10^7$ $\phi \rightarrow \eta\gamma$ generated (b).



As seen in Fig. the current CLAS results suffer from insufficient statistics. Therefore, we propose to repeat the $\eta' \rightarrow e^+e^-\gamma$ measurement with CLAS12.

4.2 Simulating and Reconstruction

To simulate the reactions in Eq. 1 and Eq. 2, the program PLUTO++ [12] was utilized for its ability to simulate the decays of those according to QED, Vector Meson Dominance or a user inputted TFF. For reconstruction of the desired topologies, the CLAS12 FASTMC was used, in which $\sim 9 \cdot 10^6$ events were generated for $\eta' \rightarrow e^+e^-\gamma$ and $\phi \rightarrow e^+e^-\eta$ and then simulated with FASTMC at 75% torus field. An extra simulation was performed for the torus field setting of 100% to show the effects of the magnetic field on the lepton acceptance. All detector efficiencies are assumed to be 100% except the EC efficiency, in which an efficiency of 10% was factored for each detected lepton. This EC efficiency was calculated with the g12 data set and the assumption is that the CLAS12 EC efficiency will be at least the same as the previous CLAS EC since the EC is the same sub-detector in both detectors.

The production of each particle was weighted by photo-production differential cross-sections, $\frac{d\sigma}{d\Omega}(v, \cos\theta_{cm})$, published in [13], where v is the virtual photon energy. This was done to achieve a quasi realistic model of the production. The e^+e^- decay spectrum, of each meson, was weighted via the VMD model (including QED predictions). Another simulation was performed using a flat $M(e^+e^-)$ distribution (No QED, No VMD) to analyze any effects of the model on the e^+e^- acceptance. The analysis showed that this acceptance was independent of the decay model, see Fig.12 and Fig.13.

4.2.1 Reconstruction And Acceptance

An exclusive reconstruction scheme

$$ep \rightarrow e'p\eta' \rightarrow pe^+e^-\gamma \quad (14)$$

$$ep \rightarrow e'p\phi \rightarrow pe^+e^-\eta, \quad (15)$$

where all final state particles are detected, as well as an inclusive reconstruction scheme

$$ep \rightarrow e'p\eta' \rightarrow e^+e^-\gamma(p) \quad (16)$$

$$(17)$$

where the proton was not detected, was analyzed. Figure 10 and Fig. 11 show the generated e^+e^- spectrum along with the accepted events for both reconstruction schemes. The acceptance was calculated by dividing the accepted events by the generated events, per $M(e^+e^-)$ bin. The η' Dalitz decay acceptance can be seen in Fig.12 and the ϕ Dalitz decay acceptance in Fig..

add reference
to plot
once
done

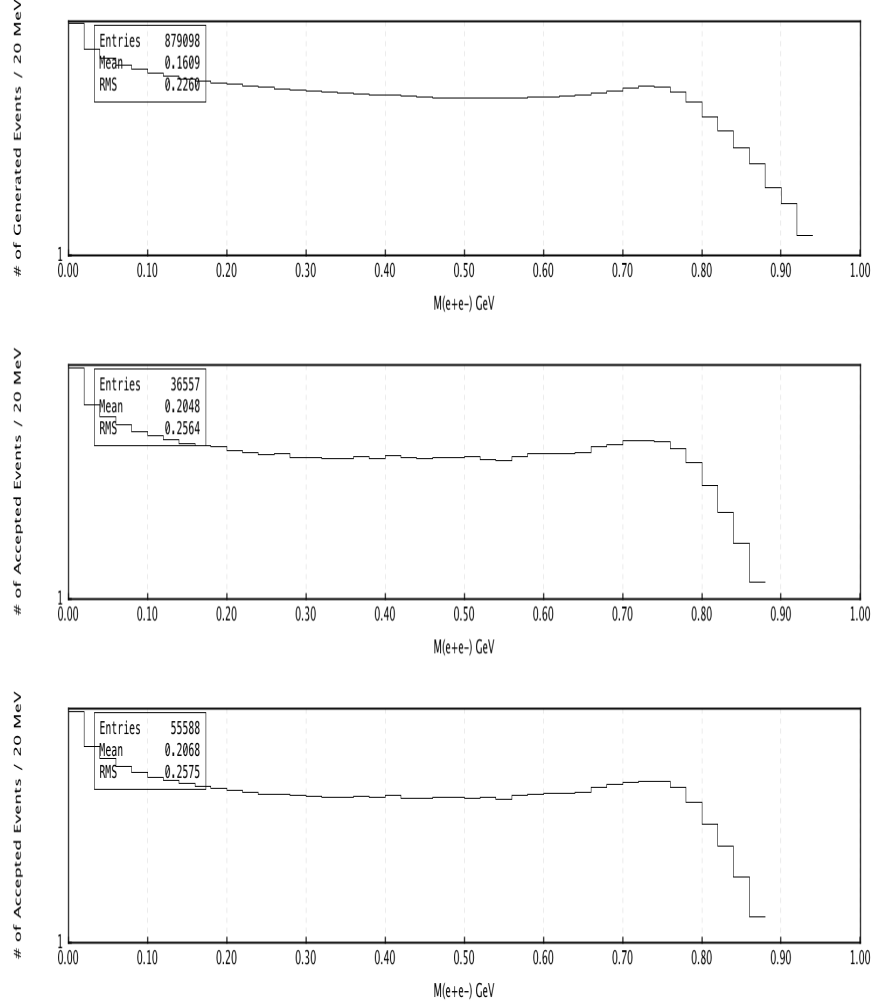


Figure 10: Generated events (Top), accepted events for an exclusive (Middle), inclusive (Bottom) reconstruction schemes as a function of $M(e^+e^-)$. In all panels a VMD decay model was employed

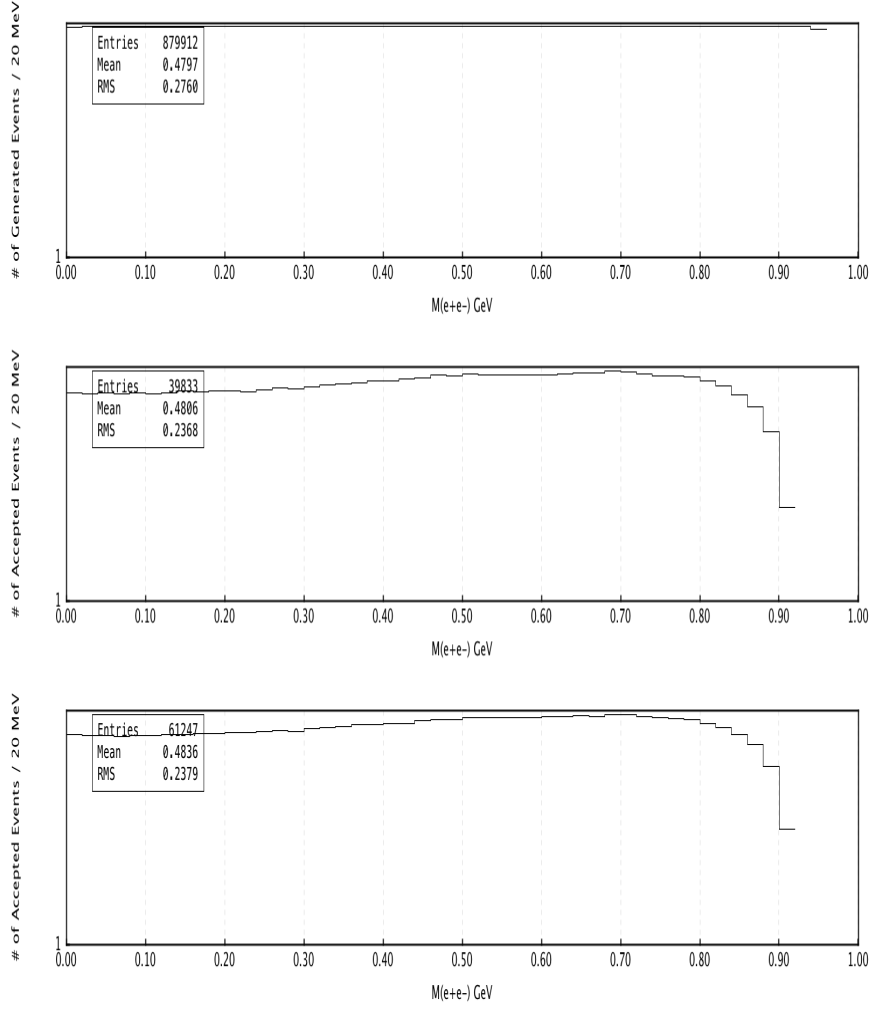


Figure 11: Generated events (Top), accepted events for an exclusive (Middle), inclusive (Bottom) reconstruction schemes as a function of $M(e^+e^-)$. In all panels a Flat e^+e^- decay model was employed

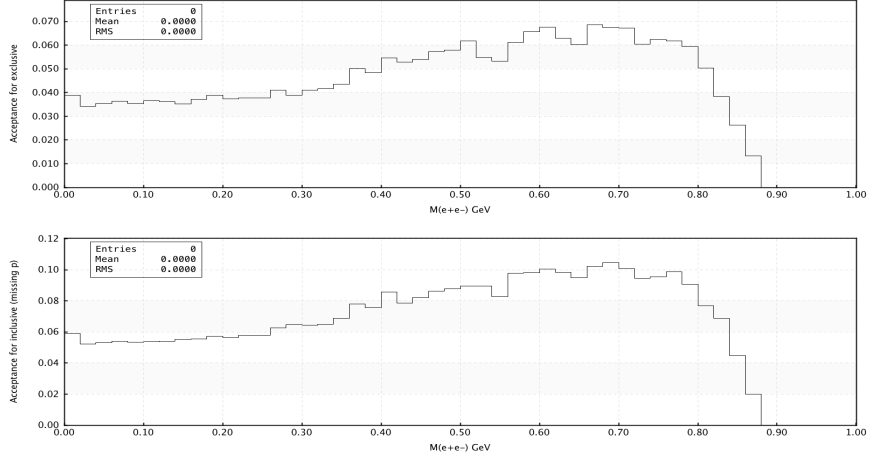


Figure 12: Acceptance using a VMD decay model, as a function of $M(e^+e^-)$ for the exclusive (Top) and inclusive reconstruction scheme(Bottom).

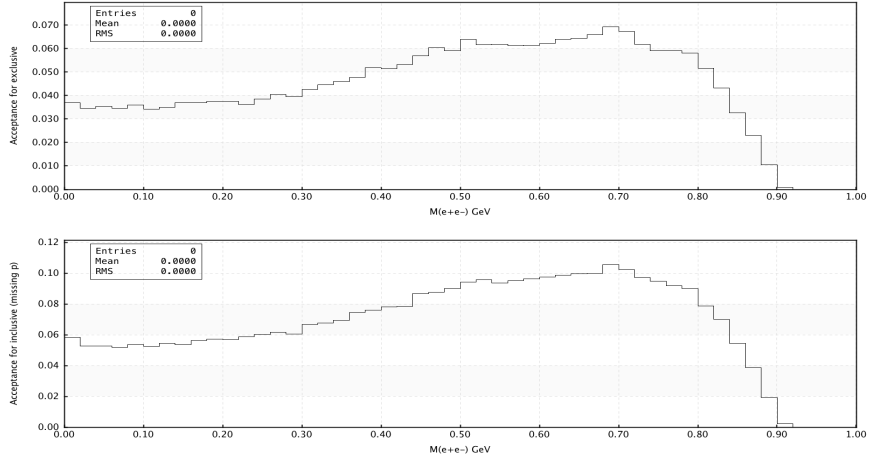


Figure 13: Acceptance using a flat e^+e^- decay model, as a function of $M(e^+e^-)$ for the exclusive (Top) and inclusive reconstruction scheme(Bottom).

4.3 Calculating Expected Yield

4.3.1 Calculating Photon Flux

A simple method for calculating the photon flux in CLAS12 is as follows; Using the fact that g12 had a photon flux of $7 \cdot 10^7$ γ/s on a Au radiator of

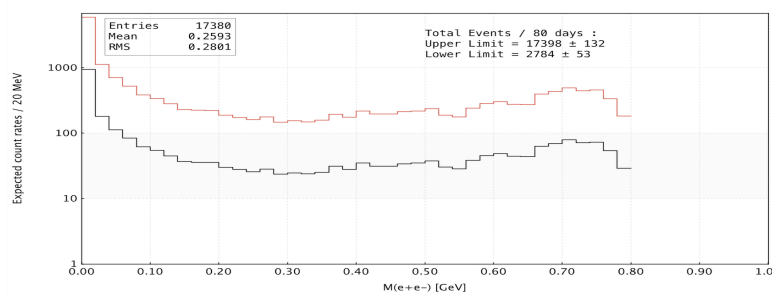
$10^{-4}\chi_0$ an expected $\sim 4 \cdot 10^9 \gamma/\text{s}$ will be seen in CLAS12 at $\mathcal{L} = 10^{35} \text{cm}^{-2} \text{s}^{-1}$ on a 5 cm ℓH_2 target which is $\sim 5.7 \cdot 10^{-3} \chi_0$. This number has been independently confirmed in a previous CLAS proposal [14].

4.3.2 Calculating Yield

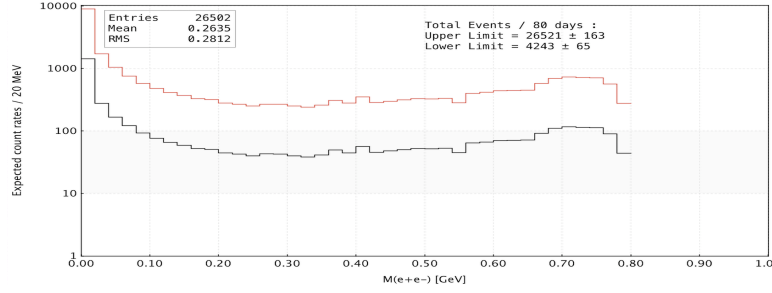
The average number of meson $\rightarrow e^+e^-X$ expected in CLAS12 can be calculated as:

$$\bar{N}(e^+e^-)_{\text{meson} \rightarrow e^+e^-X} = \Phi \epsilon(e^+e^-) \bar{\sigma} \rho_{\ell H_2} \ell_{\text{target}} N_A \frac{\Gamma_{\text{tot meson}}}{\Gamma_{\text{meson} \rightarrow e^+e^-X}}, \quad (18)$$

where Φ is the photon flux estimated in Sec. 4.3.1, ϵ is the acceptance, $\bar{\sigma}$ is the total cross-section, $\rho_{\ell H_2}$ is the atomic density of ℓH_2 , ℓ_{target} is the target length, N_A is Avogadro's constant, and $\frac{\Gamma_{\text{tot meson}}}{\Gamma_{\text{meson} \rightarrow e^+e^-X}}$ is the total branching fraction of the meson decaying into e^+e^-X . Using the lepton acceptance shown in Sec. 4.2.1 the average number of η' per $M(e^+e^-)$ can be seen in Fig. 14.



(a)



(b)

Figure 14: Count rates for the exclusive (a) and inclusive (b). For both plots the photon detection efficiency was assumed to be between 10%(Red) and 2%(Black).

Integrating over $M(e^+e^-)$, the expected yield calculates to be 17,398 events for exclusive scheme and 26,521 events for the inclusive scheme. This would increase the world statistics by a factor of ~ 20 and ~ 30 respectively. Table 1 and Tab. 2 in App. B depicts the upper and lower amount of e^+e^- expected from 80 days of beam time for two torus fields of 75% and 100% respectively.

4.4 Realistic Yield

As a reality check, lets compute the number of $\eta' \rightarrow e^+e^-\gamma$ that g12 would have seen, had the experiment ran for 80 days with a real photon flux as calculated for CLAS12 (Sec. 4.3.1). The 89 $\eta' \rightarrow e^+e^-\gamma$ events produced in g12 were recorded when the e^+e^- trigger was established. This time was

66% of the total 44 days, which is ~ 29 days. The total integrated flux measured during this time was $\sim 8.8 \cdot 10^{13}$ photons. Therefore, in 80 days the total integrated flux would have been $\sim 2.4 \cdot 10^{14}$ and the total number of $\eta' \rightarrow e^+e^-\gamma$ events recorded would have been 242. The ratio of g12 total flux at 80 days per CLAS12 real photon flux is $2.73 \cdot 10^{16}/2.4 \cdot 10^{14} \sim 114$. Therefore g12 would have recorded $114 \cdot 242 = 27590$ $\eta' \rightarrow e^+e^-\gamma$ events, which is consistent with what is proposed to be measured with 80days, in the inclusive reconstruction scheme for either torus field setting. See Sec. B for total count rates.

4.5 Acceptance at 100% Torus field

An addition simulation was performed using the same generated data shown above, the difference being the setting of the torus magnetic field. Below, in Fig. 15, the ratio of the lepton acceptance for the two different torus settings is depicted.

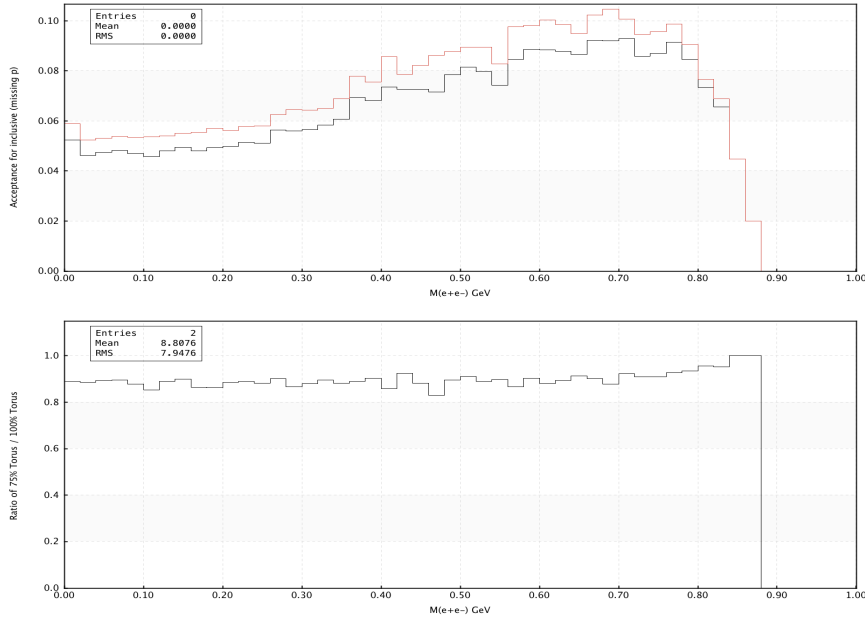


Figure 15: Acceptance using a VMD decay model, as a function of $M(e^+e^-)$ for the inclusive scheme(Top). The torus field was set to 75%(red) as well as 100%(black). Ratio of the acceptances plotted above (75%/100%)(Bottom).

5 Manpower

To analyze the $\eta' \rightarrow e^+e^-\gamma$ and $\phi \rightarrow e^+e^-\eta$ decays, a minimum of one postdoctoral associate and one graduate student will be needed to perform the following tasks:

or allotted?

- Aide in the calibration of RunGroupA
- Skim and analyze the e^+e^- data
- Simulate and correct the data
- Write publications of the results

6 Beam Time Request

With this proposal and beam time request, we ask for 100 days of beam time. Of the 100 days, 80 days will be dedicated to the production beam time with the standard CLAS setup, at full luminosity ($\sim 10^{35}\text{cm}^{-2}\text{s}^{-1}$) with 75% torus field. The remaining 20 days will be dedicated to optimizing and testing the trigger set-up (HTCC + PCAL + EC). This request should provide a competitive data sample of $\eta' \rightarrow e^+e^-\gamma$ and $\phi \rightarrow e^+e^-\eta$. The CLAS12 configuration we propose for the measurement of the transition form factors is compatible with the experimental setup already established by Run Group A.

References

- [1] R H Dalitz. On an alternative decay process for the neutral π^0 -meson. *Proceedings of the Physical Society. Section A*, 64(7):667, 1951.
- [2] J. J. Lord, Joseph Fainberg, D. M. Haskin, and Marcel Schein. Narrow angle pairs of particles from nuclear interactions. *Phys. Rev.*, 87:538–539, Aug 1952.
- [3] N. P. Samios. Dynamics of internally converted electron-positron pairs. *Phys. Rev.*, 121:275–281, Jan 1961.
- [4] P. Lindenfeld, A. Sachs, and J. Steinberger. The Internal Pair Production of γ -Rays of Mesonic Origin; Alternate Modes of π^0 Decay. *Physical Review*, 89:531–537, February 1953.
- [5] C. P. Sargent, R. Cornelius, M. Rinehart, L. M. Lederman, and K. Rogers. Diffusion cloud-chamber study of very slow mesons. i. internal pair formation. *Phys. Rev.*, 98:1349–1354, Jun 1955.
- [6] Norman M. Kroll and Walter Wada. Internal pair production associated with the emission of high-energy gamma rays. *Phys. Rev.*, 98:1355–1359, Jun 1955.
- [7] P. Stoler et al. Hard exclusive electroproduction of π^0 and η with clas12. Technical report, CLAS Analysis Proposal E12-06-108, 2011.
- [8] P. Stoler et al. Exclusive ϕ meson electroproduction with clas12. Technical report, CLAS Analysis Proposal E12-12-007, 2012.
- [9] L.G. Landsberg. Electromagnetic decays of light mesons. *Physics Reports*, 128(6):301 – 376, 1985.
- [10] M. Ablikim and et. al. Observation of the dalitz decay $\eta' \rightarrow \gamma e^+ e^-$. *Phys. Rev. D*, 92:012001, Jul 2015.
- [11] K.A. Olive et al. Review of particle physics. *Phys. Rev. C*, 38:090001, 2014.
- [12] I. Froehlich, I. Froehlich, Lorenzo Cazon, T. Galatyuk, V. Hejny, et al. Pluto: A Monte Carlo Simulation Tool for Hadronic Physics. *PoS, ACAT2007:076*, 2007.
- [13] M. Williams et al. Differential cross sections for the reactions $\gamma p \rightarrow p\eta$ and $\gamma p \rightarrow p\eta'$. *Phys. Rev. C*, 80:045213, Oct 2009.
- [14] M. Battaglieri et al. Meson spectroscopy with low q^2 electron scattering in clas12. Technical report, CLAS Analysis Proposal E12-11-005, 2010.

- [15] M.E. Peskin and D.V. Schroeder. *An Introduction to Quantum Field Theory*. Advanced book classics. Addison-Wesley Publishing Company, 1995.
- [16] F. Halzen and A.D. Martin. *Quarks and leptons: an introductory course in modern particle physics*. Wiley, 1984.
- [17] C. Hanhart, A. Kupść, U.-G. Meißner, F. Stollenwerk, and A. Wirzba. Erratum to: Dispersive analysis for $\eta \rightarrow \gamma\gamma^*$. *The European Physical Journal C*, 75(6):1–3, 2015.

Appendices

A Decay Kinematics

A.1 $\eta' \rightarrow \gamma\gamma$ Decay

As shown in Fig. 1a, the two photon decay can be expressed in terms of the respective momentum, $P_p(\eta') \rightarrow \gamma(\epsilon_1, p)\gamma(\epsilon_2, k)$, where ϵ_1 and ϵ_2 are the polarizations of the photons with 4-momenta p and k . Dropping the nomenclature (η') in $P_p(\eta')$, the four momentum of the decaying meson is $P_p = p + k$. Using the Feynman rules as given in [15] and [16], which are Lorentz and gauge invariant and also parity conserving, the amplitude can be solved to be:

$$\mathcal{M}(P_P \rightarrow \gamma(\epsilon_1, p)\gamma(\epsilon_2, k)) = M_P(p^2 = 0, k^2 = 0)\varepsilon_{\mu\nu\rho\sigma}\epsilon_1^\mu p^\nu \epsilon_2^\rho k^\sigma \quad (19)$$

where $\varepsilon_{\mu\nu\rho\sigma}$ is the antisymmetric metric tensor. The form factor, $M_P(p^2 = 0, k^2 = 0)$, contains information of the decaying meson and since the decay products are on-shell photons, which are massless, M_P is a constant given as;

$$M_P = \begin{cases} \frac{\alpha}{\pi f_\pi} & \text{if } P = \eta'; \\ \frac{\alpha}{\pi f_\pi} \frac{1}{\sqrt{3}} \left(\frac{f_\pi}{f_8} \cos \theta_{mix} - 2\sqrt{2} \frac{f_\pi}{f_0} \sin \theta_{mix} \right) & \text{if } P = \eta; \\ \frac{\alpha}{\pi f_\pi} \frac{1}{\sqrt{3}} \left(\frac{f_\pi}{f_8} \sin \theta_{mix} + 2\sqrt{2} \frac{f_\pi}{f_0} \cos \theta_{mix} \right) & \text{if } P = \eta' \end{cases} \quad (20)$$

where $\alpha = e^2/4\pi \approx 1/137$ is the fine structure constant, $f_\pi \approx 92.4 \text{ MeV}$ is the physical value of the pion-decay constant and $f_0 \approx 1.04 f_\pi$ and $f_8 \approx 1.3 f_\pi$ are the singlet and octet Pseudo-Goldstone meson decay constants.

A.1.1 Squared Matrix Element

The squared matrix element of the decay $P_P \rightarrow \gamma(\epsilon_1, p)\gamma(\epsilon_2, k)$ is given by

$$|\mathcal{M}(P_P \rightarrow \gamma(\epsilon_1, p)\gamma(\epsilon_2, k))|^2 = |M_P|^2 \varepsilon_{\mu\nu\rho\sigma} \varepsilon_{\mu'\nu'\rho'\sigma'} \epsilon_1^\mu p^\nu \epsilon_2^\rho k^\sigma \epsilon_1^{\mu'} p^{\nu'} \epsilon_2^{\rho'} k^{\sigma'} \quad (21)$$

which can be simplified to;

$$|\mathcal{M}(P_P \rightarrow \gamma(p)\gamma(k))|^2 = |M_P|^2 \varepsilon_{\mu\nu\rho\sigma} \varepsilon^{\mu\nu}_{\rho'\sigma'} p^\rho p^{\rho'} k^\sigma k^{\sigma'} \quad (22)$$

by assuming that the polarizations of the photons remain unobserved, as they are in CLAS. Therefore the photon polarization vectors can be summed

using Eq. 5.75 from [15] which reads as;

$$\sum_{\text{polarizations}} \epsilon_\mu \epsilon_{\mu'} \rightarrow -g_{\mu\mu'} \quad (23)$$

As indicated in [15], the right arrow indicates that this is not an actual equality, but the solution is valid as long as both sides are dotted into Eq. 21. The antisymmetric tensor, $\epsilon_{\mu\nu\rho\sigma}\epsilon^{\mu\nu}_{\rho'\sigma'}$ is simplified using Eq. A.30 of [15];

$$\epsilon_{\mu\nu\rho\sigma}\epsilon^{\mu\nu}_{\rho'\sigma'} = -2(g_{\rho\rho'}g_{\sigma\sigma'} - g_{\rho\sigma'}g_{\rho'\sigma}) \quad (24)$$

$$(25)$$

Applying Eq. 24 to Eq. 22 results in;

$$|\mathcal{M}(P_P \rightarrow \gamma(p)\gamma(k))|^2 = |M_P|^2 (-2)(p^2 k^2 - (p \cdot k)^2) . \quad (26)$$

Substituting

$$(p + k)^2 = p^2 + k^2 + 2(p \cdot k) , \quad (27)$$

and applying $p^2 = k^2 = 0$, since both photons are massless because they are on-shell, we can derive the final expression of the squared amplitude of the decay $P_P \rightarrow \gamma(\epsilon_1, p)\gamma(\epsilon_2, k)$ as;

$$|\mathcal{M}(P_P \rightarrow \gamma(p)\gamma(k))|^2 = |M_P|^2 \frac{1}{2}(p + k)^4 = \frac{1}{2} |M_P|^2 m_P^4 \quad (28)$$

where m_P^4 is the mass of the η' derived from the 4-momenta conservation equation $(p + k)^4 = m_P^4$

A.1.2 Decay rate

The decay rate of a two-body decay is explained in Equation 46.17 of [11] as

$$d\Gamma = \frac{1}{32\pi^2} A |\mathcal{M}|^2 \frac{|\mathbf{p}_1|}{m_p^2} d\Omega , \quad (29)$$

where $d\Omega$ is the solid angle of particle 1 and A is the symmetry factor which appears because of the Bose symmetry of the two outgoing photons. Substituting the square matrix element from Eq. 28 into Eq. 29 and integrating over the solid angle yields;

$$\Gamma_{P \rightarrow \gamma\gamma} = \frac{1}{32\pi^2} \frac{1}{2} |\mathcal{M}(P_P \rightarrow \gamma(p)\gamma(k))|^2 \frac{|\mathbf{p}|}{m_P^2} 4\pi = \frac{1}{32\pi} |M_P|^2 m_P^2 |\mathbf{p}| \quad (30)$$

Finally, in the center-of-mass (C.M.) frame of the decaying meson, $\mathbf{p} = \mathbf{E}_\gamma^{\text{C.M.}} = \frac{m_P}{2}\mathbf{p}$, we find the final expression of the decay rate of $P_P \rightarrow \gamma(\epsilon_1, p)\gamma(\epsilon_2, k)$ as;

$$\Gamma_{P \rightarrow \gamma\gamma} = \frac{1}{64\pi} |M_P|^2 m_P^3 . \quad (31)$$

A.2 $\phi \rightarrow \eta\gamma$ Decay

The $\phi \rightarrow \eta\gamma$ decay is analogous to the $\eta' \rightarrow \gamma\gamma$ decay by replacing the initial pseudoscalar meson P_p with a vector meson V_p and one of the γ propagators with η . In this substitution

$$\mathcal{M}(V_P(\epsilon_1) \rightarrow \eta(p)\gamma(\epsilon_2, k)) = M_V(p^2 = m_\eta, k^2 = 0)\epsilon_{\mu\nu\rho\sigma}\epsilon_1^\mu p^\nu \epsilon_2^\rho k^\sigma \quad (32)$$

again, $\epsilon_{\mu\nu\rho\sigma}$ is the antisymmetric metric tensor and the form factor, $M_V(p^2 = m_\eta, k^2 = 0)$, contains information of the $\phi - \eta$ transition.

A.2.1 Decay rate

The algebra for solving the squared matrix element is similar to Sec. A.1.1, however since now the initial meson has polarization, a factor of $1/3$ [17] is introduced. The decay rate is also similar within a factor of $1/3$ and can be represented as:

$$\Gamma_{V \rightarrow \eta\gamma} = \frac{1}{3} \frac{1}{64\pi} |M_V|^2 \left(\frac{m_\phi - m_\eta}{m_\phi} \right)^3. \quad (33)$$

A.3 η' Dalitz Decay

When a pseudoscalar meson decays via a photon γ and a dilepton (l^+l^-) pair, it is known as a Dalitz decay or a so-called single off-shell decay. The Dalitz decay is related to the two photon decay. However, in the Dalitz decay, one of the photons is off-shell (γ^*) and decays into a dilepton pair. Since the Dalitz decay is related to the two photon decay, the form factor of the Dalitz decay, for $P(\eta')$, will be similar to the form factor of the two photon decay of $P(\eta')$, except there will be an effective mass dependence for the Dalitz decay. Figure 1b depicts the Feymann diagram of the Dalitz decay.

The amplitude for the decay $P_P \rightarrow \gamma^*(p)\gamma(k) \rightarrow l^+(p_+)l^-(p_-)\gamma(k)$ is given by the following expression:

$$\mathcal{M}(P \rightarrow l^+(p_+, s_+)l^-(p_-, s_-)\gamma) = M_P(p^2, k^2 = 0)\epsilon_{\mu\nu\rho\sigma}\frac{1}{q^2}e\bar{u}(p_-, s_-)\gamma^\mu v(p_+, s_-)q^\nu \epsilon^\rho k^\sigma. \quad (34)$$

Comparing the amplitudes of Eq. 34 and Eq. 19 it is seen that the polarization of the off-shell photon turned into the current $e\bar{u}(p_-, s_-)\gamma^\mu v(p_+, s_-)$ of the lepton pair. The parameters s_\pm are the spin helicities of the outgoing leptons l^\pm and as in Eq. 21, ϵ is the polarization of the outgoing photon.

A.3.1 Squared Matrix Element

$$|\mathcal{M}(P \rightarrow l^+(p_+, s_+) l^-(p_-, s_-) \gamma)|^2 = \frac{e^2}{q^4} |M|^2 \varepsilon_{\mu\nu\rho\sigma} \varepsilon_{\mu'\nu'\rho'\sigma'} \bar{u}(p_-, s_-) \gamma^\mu v(p_+, s_+) \bar{v}(p_+, s_+) \gamma^{\mu'} u(p_-, s_-) q^\nu \epsilon^\rho k^\sigma q^{\nu'} \epsilon^{\rho'} k^{\sigma'}. \quad (35)$$

using an equation found between equation 5.3 and 5.4 found in [15]

$$\sum_{s_-, s_+} \bar{u}(p_-, s_-) \gamma^\mu v(p_+, s_+) \bar{v}(p_+, s_+) \gamma^{\mu'} u(p_-, s_-) = \text{Tr} \left[(\not{p}_- + m) \gamma^\mu (\not{p}_+ - m) \gamma^{\mu'} \right] \\ = 2q^2 \left[-(g_{\mu\mu'} - \frac{p_\mu p_{\mu'}}{q^2}) - \frac{(p_+ - p_-)_\mu (p_+ - p_-)_{\mu'}}{q^2} \right] \quad (36)$$

where the identity $q = p_+ + p_-$ was used. Substituting Eq. 36 into Eq. 35

$$|\mathcal{M}|^2 = \frac{2e^2 |M_P|^2}{q^2} \varepsilon_{\mu\nu\rho\sigma} \varepsilon_{\mu'\nu'\rho'\sigma'} \left[-g^{\mu\mu'} - \frac{(p_+ - p_-)^\mu (p_+ - p_-)^{\mu'}}{q^2} \right] (-g^{\nu\nu'}) q^\rho k^\sigma q^{\rho'} k^{\sigma'} \quad (37)$$

Substituting $k = P - q$ and $p_- = q - p_+$ into Eq. 37

$$|\mathcal{M}|^2 = \frac{2e^2 |M_P|^2}{q^2} \varepsilon_{\mu\nu\rho\sigma} \varepsilon_{\mu'\nu'\rho'\sigma'} \left[-g^{\mu\mu'} - \frac{(2p_+ - q)^\mu (2p_+ - q)^{\mu'}}{q^2} \right] \\ \times (-g^{\nu\nu'}) (q^\rho P^\sigma - q^\rho q^\sigma) (q^{\rho'} P^{\sigma'} - q^{\rho'} q^{\sigma'}) \quad (38)$$

Applying properties of $-g^{\mu\mu'}$ and $-g^{\nu\nu'}$ onto Eq. 38

$$|\mathcal{M}|^2 = \frac{2e^2 |M_P|^2}{q^2} \left[\varepsilon_{\mu\nu\rho\sigma} \varepsilon^{\mu\nu}_{\rho'\sigma'} q^\rho P^\sigma q^{\rho'} P^{\sigma'} + \frac{4}{q^2} \varepsilon_{\mu\nu\rho\sigma} \varepsilon^\mu_{\nu'\rho'\sigma'} p_+^\nu p_+^{\nu'} q^\rho q^{\rho'} P^\sigma P^{\sigma'} \right] \quad (39)$$

Switching to the rest frame of the pseudoscalar meson, P_p , the 4-momenta is transformed to $P^\sigma = m_p \delta^{\sigma 0}$. The squared amplitude of Eq. 39 reads;

$$|\mathcal{M}|^2 = \frac{2e^2 |M_P|^2}{q^2} m_p^2 \left[\varepsilon_{\mu\nu\rho} \varepsilon^{\mu\nu}_{\rho'} q^\rho q^{\rho'} - \frac{4}{q^2} \varepsilon_{\mu\nu\rho} \varepsilon^\mu_{\nu'\rho'} p_+^\nu p_+^{\nu'} q^\rho q^{\rho'} \right] \quad (40)$$

The sign change is due to $g^{\sigma\sigma'} = -\delta^{\sigma\sigma'}$. Using the antisymmetric tensor properties $\varepsilon_{\mu\nu\rho} \varepsilon^{\mu\nu}_{\rho'} = 2\delta_{\rho\rho'}$ and $\varepsilon_{\mu\nu\rho} \varepsilon^\mu_{\nu'\rho'} = \delta_{\nu\nu'} \delta_{\rho\rho'} - \delta_{\nu\rho'} \delta_{\rho\nu'} = (\hat{e}_\nu \times \hat{e}_\rho) \cdot (\hat{e}_{\nu'} \times \hat{e}_{\rho'})$, Eq. 40 is reduced to

$$|\mathcal{M}|^2 = \frac{2e^2 |M_P|^2}{q^2} m_p^2 \left[2|\mathbf{q}|^2 - \frac{4}{q^2} |\mathbf{q}|^2 |\mathbf{p}_+|^2 \sin^2(\theta_{p_+q}) \right] \quad (41)$$

A.3.2 Decay rate

The decay rate of a three-body decay is given in Equation 46.19 of [11] as

$$d\Gamma = \frac{1}{(2\pi)^5} \frac{1}{16m_p^2} |\mathcal{M}|^2 |\mathbf{p}_1^*| |\mathbf{p}_3| d\Omega_1^* d\Omega_3 dm_{12} , \quad (42)$$

where $(|\mathbf{p}_1^*|, \Omega_1^*)$ is the momentum of particle 1 in the rest frame of 1 and 2, and Ω_3 is the angle of particle 3 in the rest frame of the decaying particle m_p [11]. Relating Eq. 42 to the variables in Eq. 41, where $(|\mathbf{p}_1^*|, \Omega_1^*) = (|\mathbf{p}_+|, \Omega_{p_+q})$, $m_{12} = q$ and $(|\mathbf{p}_3|, \Omega_3) = (|\mathbf{p}_k|, \Omega_k)$, reads;

$$d\Gamma = \frac{1}{(2\pi)^5} \frac{1}{16m_p^2} |\mathcal{M}|^2 |\mathbf{p}_+| |\mathbf{p}_k| d\Omega_+ d\Omega_k dq , \quad (43)$$

In the rest frame of the decaying particle m_p , the 3-momenta $|\mathbf{p}_k| = |\mathbf{q}|$ and the solid angle $\Omega_k = \Omega_q$. Substituting the square matrix element from Eq. 41 into Eq. 43 yields;

$$d\Gamma = \frac{1}{(2\pi)^5} \frac{1}{16m_p^2} \frac{2e^2 |M_P|^2}{q^2} m_p^2 \left[2|\mathbf{q}|^2 - \frac{4}{q^2} |\mathbf{q}|^2 |\mathbf{p}_+|^2 \sin^2(\theta_{p_+q}) \right] |\mathbf{p}_+| |\mathbf{q}| d\Omega_{p_+q} d\Omega_q dq . \quad (44)$$

The variables $|\mathbf{q}|$ and $|\mathbf{p}_+|$ can be redefined, by means of Eq. 46.20b and Eq. 46.20a of [11], as

$$|\mathbf{q}| = \frac{m_p^2 - q^2}{2m_p} \quad (45)$$

$$|\mathbf{p}_+| = \frac{\sqrt{q^2 - 4m_l^2}}{2} = \frac{q\sqrt{1 - \frac{4m_l^2}{q^2}}}{2} = \frac{q\mathcal{K}}{2} , \quad (46)$$

where $\mathcal{K} = \sqrt{1 - \frac{4m_l^2}{q^2}}$. Replacing the variables calculated in Eq. 45 and Eq. 46 into Eq. 44 and collecting terms yields;

$$d\Gamma = \frac{1}{(2\pi)^5} \frac{1}{16m_p^2} |M_P|^2 \left[\frac{2e^2 m_p^2}{8} \left(\frac{m_p^2 - q^2}{2m_p} \right)^3 \right] \left(2 - \mathcal{K}^2 \sin^2(\theta_{p_+q}) \right) \frac{\mathcal{K}}{4q^2} dq^2 d\Omega_{p_+q} d\Omega_q , \quad (47)$$

where the identity $qdq = \frac{dq^2}{2}$. Performing the integration of $\Omega_{p_+q} d\Omega_q$ and replacing $e^2 = 4\pi\alpha$ transforms Eq. 47 into;

$$d\Gamma = \frac{1}{(2\pi)^3} \frac{1}{32} \frac{4\pi\alpha}{3} |M_P|^2 \left[\frac{m_p^6 \left(1 - \frac{q^2}{m_p^2} \right)^3}{m_p^3} \right] (3 - \mathcal{K}^2) \frac{\mathcal{K}}{q^2} dq^2 , \quad (48)$$

which can be simplified further to;

$$d\Gamma = \left(\frac{1}{64\pi} |M_P|^2 m_P^3 \right) \frac{2\alpha}{3\pi} \frac{1}{q^2} \left(1 - \frac{q^2}{m_p^2} \right)^3 \left(1 + \frac{2m_l^2}{q^2} \right) \left(1 - \frac{4m_l^2}{q^2} \right)^{\frac{1}{2}} dq^2 . \quad (49)$$

It can be seen that the first set of variables in parenthesis in Eq. 49 is Eq. 31, therefore;

$$\frac{d\Gamma}{\Gamma_{\gamma\gamma} dq^2} = \frac{2\alpha}{3\pi} \frac{1}{q^2} \left(1 - \frac{q^2}{m_p^2} \right)^3 \left(1 + \frac{2m_l^2}{q^2} \right) \left(1 - \frac{4m_l^2}{q^2} \right)^{\frac{1}{2}} \quad (50)$$

which is the Kroll-Wada equation founded in [6].

A.4 ϕ Dalitz Decay

The amplitude for the decay $V_P \rightarrow \gamma^*(p_1)\eta(p_2) \rightarrow l^+(p_+)l^-(p_-)\eta(p_2)$ is similar Eq. 34, but replacing the on-shell photon with an η :

$$\mathcal{M}(P \rightarrow l^+(p_+, s_+)l^-(p_-, s_-)\eta(p_2)) = M_P(p_1^2, p_2^2)\varepsilon_{\mu\nu\rho\sigma}\frac{1}{q^2}e\bar{u}(p_-, s_-)\gamma^\mu v(p_+, s_+)q^\nu\epsilon^\rho p_2^\sigma. \quad (51)$$

A.4.1 Decay rate

The decay rate for the ϕ transition to $\eta\gamma^*$ is derived as [9]:

$$\frac{d\Gamma}{\Gamma_{\eta\gamma} dq^2} = \frac{\alpha}{3\pi} \frac{1}{q^2} \left(\left(1 + \frac{q^2}{m_\phi^2 - m_\eta^2} \right)^2 - \frac{4m_\phi^2 q^2}{m_\phi^2 - m_\eta^2} \right)^{\frac{3}{2}} \left(1 + \frac{2m_l^2}{q^2} \right) \left(1 - \frac{4m_l^2}{q^2} \right)^{\frac{1}{2}} , \quad (52)$$

B Tabular Rates

Table 1 gives expected count rate for several bins of $M(e^+e^-)$ for a torus field setting of 75%. Table 2 gives expected count rate for several bins of $M(e^+e^-)$ for a torus field setting of 100%.

| $M(e^+e^-)$ Bin Center | Upper | Uncertainty | Lower | Uncertainty |
|------------------------|-------|-------------|-------|-------------|
| 0.01 | 8924 | 94 | 946 | 31 |
| 0.03 | 1720 | 41 | 180 | 13 |
| 0.05 | 1041 | 32 | 113 | 11 |
| 0.07 | 758 | 28 | 84 | 9 |
| 0.09 | 578 | 24 | 62 | 8 |
| 0.11 | 479 | 22 | 54 | 7 |
| 0.13 | 411 | 20 | 45 | 7 |
| 0.15 | 369 | 19 | 37 | 6 |
| 0.17 | 329 | 18 | 36 | 6 |
| 0.19 | 317 | 18 | 36 | 6 |
| 0.21 | 280 | 17 | 30 | 5 |
| 0.23 | 268 | 16 | 28 | 5 |
| 0.25 | 250 | 16 | 26 | 5 |
| 0.27 | 269 | 16 | 28 | 5 |
| 0.29 | 266 | 16 | 24 | 5 |
| 0.31 | 250 | 16 | 25 | 5 |
| 0.33 | 240 | 15 | 24 | 5 |
| 0.35 | 258 | 16 | 25 | 5 |
| 0.37 | 309 | 18 | 31 | 6 |
| 0.39 | 280 | 17 | 28 | 5 |
| 0.41 | 352 | 19 | 35 | 6 |
| 0.43 | 285 | 17 | 31 | 6 |
| 0.45 | 299 | 17 | 31 | 6 |
| 0.47 | 315 | 18 | 34 | 6 |
| 0.49 | 328 | 18 | 35 | 6 |
| 0.51 | 326 | 18 | 38 | 6 |
| 0.53 | 331 | 18 | 30 | 5 |
| 0.55 | 282 | 17 | 28 | 5 |
| 0.57 | 401 | 20 | 38 | 6 |
| 0.59 | 416 | 20 | 45 | 7 |
| 0.61 | 438 | 21 | 48 | 7 |
| 0.63 | 445 | 21 | 44 | 7 |
| 0.65 | 448 | 21 | 44 | 7 |
| 0.67 | 577 | 24 | 63 | 8 |
| 0.69 | 689 | 26 | 69 | 8 |
| 0.71 | 728 | 27 | 79 | 9 |
| 0.73 | 716 | 27 | 71 | 8 |
| 0.75 | 706 | 27 | 73 | 9 |
| 0.77 | 565 | 24 | 54 | 7 |
| 0.79 | 277 | 17 | 29 | 5 |
| Total | 26521 | 163 | 2784 | 53 |

Table 1: Counts rates for bins of $M(e^+e^-)$ at 75% torus field

| $M(e^+e^-)$ Bin Center | Upper | Uncertainty | Lower | Uncertainty |
|------------------------|-------|-------------|-------|-------------|
| 0.01 | 7937 | 89 | 859 | 29 |
| 0.03 | 1516 | 39 | 163 | 13 |
| 0.05 | 934 | 31 | 102 | 10 |
| 0.07 | 684 | 26 | 77 | 9 |
| 0.09 | 501 | 22 | 56 | 7 |
| 0.11 | 392 | 20 | 45 | 7 |
| 0.13 | 366 | 19 | 40 | 6 |
| 0.15 | 335 | 18 | 34 | 6 |
| 0.17 | 276 | 17 | 31 | 6 |
| 0.19 | 266 | 16 | 30 | 5 |
| 0.21 | 246 | 16 | 28 | 5 |
| 0.23 | 238 | 15 | 25 | 5 |
| 0.25 | 218 | 15 | 22 | 5 |
| 0.27 | 245 | 16 | 26 | 5 |
| 0.29 | 225 | 15 | 21 | 5 |
| 0.31 | 218 | 15 | 22 | 5 |
| 0.33 | 217 | 15 | 22 | 5 |
| 0.35 | 226 | 15 | 23 | 5 |
| 0.37 | 275 | 17 | 29 | 5 |
| 0.39 | 256 | 16 | 27 | 5 |
| 0.41 | 292 | 17 | 31 | 6 |
| 0.43 | 274 | 17 | 29 | 5 |
| 0.45 | 262 | 16 | 26 | 5 |
| 0.47 | 244 | 16 | 27 | 5 |
| 0.49 | 296 | 17 | 32 | 6 |
| 0.51 | 303 | 17 | 36 | 6 |
| 0.53 | 295 | 17 | 28 | 5 |
| 0.55 | 255 | 16 | 26 | 5 |
| 0.57 | 338 | 18 | 33 | 6 |
| 0.59 | 381 | 20 | 43 | 7 |
| 0.61 | 382 | 20 | 43 | 7 |
| 0.63 | 399 | 20 | 41 | 6 |
| 0.65 | 419 | 20 | 41 | 6 |
| 0.67 | 527 | 23 | 57 | 8 |
| 0.69 | 597 | 24 | 62 | 8 |
| 0.71 | 695 | 26 | 76 | 9 |
| 0.73 | 664 | 26 | 68 | 8 |
| 0.75 | 657 | 26 | 68 | 8 |
| 0.77 | 545 | 23 | 54 | 7 |
| 0.79 | 271 | 16 | 28 | 5 |
| Total | 23667 | 154 | 2528 | 50 |

Table 2: Counts rates for bins of $M(e^+e^-)$ at 100% torus field